Albumen Transport to Bruch's Membrane and RPE by Choriocapillaris Caveolae

Masataka Nakanishi, Rhonda Grebe, Imran A. Bhutto, Malia Edwards, D. Scott McLeod, and Gerard A. Lutty

Wilmer Eye Institute, Johns Hopkins University School of Medicine, Baltimore, Maryland, United States

Correspondence: Gerard A. Lutty, G. Edward and G. Britton Durell Professor of Ophthalmology, M041 Smith Building, Wilmer Ophthalmological Institute, Johns Hopkins Hospital, 400 N. Broadway, Baltimore, MD 21287, USA; glutty@jhmi.edu.

Submitted: August 12, 2015
Accepted: March 20, 2016

Citation: Nakanishi M, Grebe R, Bhutto IA, Edwards M, McLeod DS, Lutty GA. Albumen transport to Bruch's membrane and RPE by choriocapillaris caveolae. *Invest Ophthalmol Vis Sci.* 2016;57:2213–2224. DOI:10.1167/iovs.15-17934

Purpose. The choriocapillaris (CC), the capillary network of the choroid, is positioned adjacent to Bruch's membrane (BM) and the RPE. The aim of this study was to clarify the mechanism(s) for transport of serum albumen from CC lumen to RPE.

Methods. Alexa647 conjugated to BSA (BSA-A647) or PBS was administrated via the femoral vein to young and aged wild-type (WT; C57BL/6J) mice and Caveolin-1 knockout mice (*Cav1*$^{-/-}$). Mice were perfused with PBS and killed at 30 minutes, 1 hour, and 4 hours after injection. Eyecups were cryopreserved, and cryosections were analyzed on a Zeiss 710 confocal microscope. Bovine serum albumin conjugated to gold nanoparticles (BSA-GNP) was administrated through the left common carotid artery. Mice were perfused with PBS and killed at 30 minutes after injection. Eyecups were embedded after fixation, and 70-nm-thick sections were analyzed on a Hitachi H7600 transmission electron microscope.

Results. In eyes of WT young mice, BSA-A647 was transported to the RPE at 30 minutes and diffused to the photoreceptor layer by 1 hour. In contrast, most BSA-A647 was found in the CC in *Cav1*$^{-/-}$ eyes. The majority of BSA-GNP found in the CC of young WT mice was on the luminal side in caveolae at 30 minutes after injection. In aged WT mice, BSA-GNPs were found in defective tight junctions between endothelial cells and appeared trapped at the diaphragm of fenestrations.

Conclusions. Normally, CC carefully regulates transport system of BSA from lumen to BM by caveolae-mediated transcytosis; however, endothelium cells of aged control WT mice have leaky tight junctions and lacked regulated BSA transport.

Keywords: age-related macular degeneration, albumen, caveolae, Cav1, choriocapillaris, choroid, fenestrations

The capillary system of choroid, the choriocapillaris (CC), is unique in structure and function. It is positioned adjacent to the RPE monolayer and separated from the RPE by Bruch's membrane (BM). It has a lobular architecture and is fenestrated predominantly on the retinal side of the vascular lumen. The choroidal vasculature provides all of the exogenous nutrients and oxygen for the RPE cells and highly metabolically active photoreceptors.[1] If the CC becomes dysfunctional and blood flow is compromised, photoreceptors are deprived of nutrients and oxygen, potentially leading to their degeneration. What nutrients the CC transports and how this is accomplished is not known. It is assumed that the fenestrations provide rapid transport of solutes and small molecules into and out of the CC.[2] However, transport of macromolecules probably occurs by the caveolae system or via coated pits, and these transport systems have never been critically evaluated in CC. Only fenestrations have been studied historically in the normal mammalian CC. A common misconception is that CC, being fenestrated, allows free transport of macromolecules to RPE when in actuality the endothelial cells of CC have tight junctions and carefully regulate the transport of material from lumen to the RPE and vice versa.

Transcytosis systems of endothelium cells (ECs) have been studied extensively in kidney and liver but only cursorily in CC.[3–6] There are several possible mechanisms for physiologic transport of macromolecules across a capillary wall: caveolae, which are 60–80 nm in diameter; vesiculo-vacuolar organelles (VVOs), 0.12–0.14 mm^2; transendothelial channels (TECs); and fenestrations (60- to 80-nm pores).[6–8] Caveolae (or plasmalemma vesicles) are responsible for transport of macromolecules like albumen in EC systems (Table). The VVOs and TECs are thought by some to be assemblies of caveolae that transport large macromolecules like ferritin transcellularly,[9] whereas others question the relation of TECs to caveolae.[6]

From studies in liver and kidney, a few molecules have been isolated and characterized that are important in transport through fenestrations and caveolae: plasmalemmal vesicle-associated protein-1 (PV-1) and the caveolins (Cavs). There are now three Cavs known, but Cav-1 seems to be most important in EC transcytosis.[10] Caveolin-1 is a cholesterol-binding protein, and genetic ablation of Cav-1 eliminated caveolae but not VVO or TEC formation.[6]

Fenestrations are responsible for rapid transport of solutes and small molecules (Table). The type of fenestration (diaphragm or not) and size are unique in each organ system.[11] Fenestrations vary in pore size from 60 to 80 nm with diaphragms (e.g., CC; Table) to 100 to 175 nm in liver and 60 to 80 nm in kidney glomeruli; the latter two organs have fenestrations without diaphragms in normal adults.[11] In kidney, fenestrations restrict protein passage into urine, which appears

Table. Transport Systems of CC

Transport System	Pore Size or Opening	Transport Method	Transported Material (MW)
Fenestrations with diaphragms	60- to 80-nm pore divided by diaphragm predicted 6-nm opening	Diffusion	Inulin (5.5 kDa)[42] Vitamin B12 (1.3 kDa)[43,44] Water ≤5-nm-d molecules[42] <3.2-nm ESR[2,19]
Caveolae	Invagination 60–80 nm	Receptor-mediated transcytosis and intracellular transport[9,33]	Albumin (68 kDa; 3.48-nm ESR)[21] LDL[9] Transthyretin (55 kDa)[45] PDGF[9] Insulin (6 kDa)[9] eNOS[9] Transferrin (80 kDa)[7]
Transendothelial channels	Invagination 60–80 nm	Receptor-mediated transcytosis	Transthyretin[45] Transferrin[7] LDL[7] Albumen Insulin[7]
Coated pits	Invagination 60–80 nm	Receptor-mediated endocytosis to lysosomes	LDL (18- to 28-nm-d)[46]

d, diameter; ESR, Einstein Stokes radius; intracellular transport, to Golgi and endoplasmic reticulum or lysozomes; MW, molecular weight in kilodaltons; PDGF, platelet-derived growth factor; eNOS, endothelial nitric oxide synthase.

to be accomplished in part by the glycocalyx that covers the channel opening.[12,13] In kidney development and in pathologic states, diaphragms are present in fenestrations, but diaphragms are not present in normal adult kidney.[14] Plasmalemmal vesicle-associated protein-1 is a major component of the diaphragms in fenestrations and some caveolae.[15,16] Macromolecules could also cross the CC via leakage through open tight junctions (TJs). Although CC is fenestrated, it also has TJs like other vascular endothelium to restrict nonspecific passage of macromolecules. In disease states like diabetes, there is loss of TJs between retinal EC resulting in leakage of serum proteins out of the vascular system and into interstitial spaces resulting in hard and soft exudates.[17]

A detailed description of the CC transport systems has never been undertaken, and the last attempt was in the 1980s by Pino et al., before the caveolae system was even known. Pino et al. used a series of proteins (horseradish peroxidase [HRP, 40 kDa], hemoglobin [68 kDa], lactoperoxidase [84 kDa], catalase [240 kDa], ferritin [480 kDa]) and found that only HRP traversed the CC and was found in BM and RPE cells.[18–23] Most of the tracers used by Pino et al. were biologically active macromolecules that could have exerted their own effect on transport properties, and they evaluated transport for 30- and 60-minute time points after injection only. Since those pioneering studies, very little information on CC transport has been elucidated.

The present study evaluates the mechanisms for EC transcytosis of BSA from lumen to RPE in young and aged mice. It is important to understand normal CC transport mechanisms and its regulation so we can determine whether alteration of transport contributes to disease states like AMD. For these studies, BSA was conjugated to Alexafluor-647 to evaluate transport at the tissue or light level using the confocal microscope and conjugated to gold nanoparticles (GNPs) to evaluate albumen in subcellular compartments and structures like caveolae and fenestrations. Our central hypothesis is that the fenestrations, coated pits, and caveolae of CC control the flux of materials from serum to BM and RPE, and regulation of that transport changes with age. Cav1$^{-/-}$ mice were used to evaluate the effect of caveolae deficiency. Dysfunction in CC transport could result in loss of nutrient supply to RPE and photoreceptors.

Materials and Methods

Animals

All animal experiments were conducted in accordance with the ARVO Statement for the Use of Animals in Ophthalmic and Vision Research and the guidelines of the University of Johns Hopkins Animal Care and Use Committee. The mice used were C57BL/6J mice (B6 or wild type [WT]) and caveolin-1 knockout mice (*Cav1*$^{-/-}$), strain B6.Cg-Cav1^{tm1Mls}/J from the Jackson Laboratory (Bar Harbor, ME, USA), which are caveolae deficient. Mice were used at 3 and 14 months of age.

Preparation of Tracers

Bovine serum albumen was used in the native form or labeled with Alexa Fluor 647 (A647; Molecular Probes, Eugene, OR, USA), following the instructions of the manufacturer. Purification was performed by dialysis (MWCO 20,000; Spectra Labs, Inc., Rancho Dominguez, CA, USA) against deionized water three times for 3 hours each. Free dye was successfully removed, which was confirmed by HPLC using an Acquity UPLC BEH300 C4 column (Waters, San Antonio, TX, USA): eluent A: 0.1% trifluoroacetic acid (TFA) in water, eluent B: 0.1% TFA in acetonitrile, flow rate of 0.2 mL/min, and gradient of eluent A to eluent B over 30 minutes (Supplementary Fig. S1).

Gold-albumen conjugates (BSA-GNP) were prepared as follows. The 5-nm GNP (Ted Pella, Inc., Redding, CA, USA) solution was first filtered through a 0.2-mm Gelman membrane (Ann Arbor, MI, USA) and then equally mixed with a 0.01 mM BSA solution. The mixture was stirred for 1 hour and then incubated at 41°C for 24 hours to facilitate BSA-GNP conjugation. The BSA-GNP was condensed 10 times by centrifugation at 13,700*g* for 3 hours. Size and zeta-potential or surface charge of the synthesized BSA-GNP were determined by Zeta-sizer (Malvern, Westborough, MA, USA; Supplementary Fig. S2). The morphology of the synthesized BSA-GNP conjugate was characterized with an H-7600 transmission

Investigative Ophthalmology & Visual Science

electron microscope (TEM) (Hitachi High-Technologies, Tarrytown, NY, USA; Supplementary Fig. S3).

Uptake of BSA In Vitro

Human umbilical vein endothelial cells (HUVECs) were seeded in 24-well culture plates at a density of 5×10^4 cells per well in 400 μL medium, followed by incubation with 10 μL BSA-A647 (6 μg Alexa647) or A647 dye/NaOH solution (pH 9, 6 μg Alexa674) for 60 minutes in medium containing 10% fetal bovine serum (FBS) without antibiotics. Culture medium was removed, and the cells were washed with cold PBS and then fixed in 2% paraformaldehyde in PBS for fluorescent imaging.

Administration of Tracers In Vivo

Bovine serum albumin–A647 was injected intravenously through a femoral vein. Mice were anesthetized with 0.15 mL ketamine/xylazine (10 mg/mL ketamine/2 mg/mL xylazine) intraperitoneal (IP). The BSA-A647 solution, equivalent to 0.6 mg BSA in 200 μL, was administrated by manual injection and given for the determined time intervals, and then animals were killed by sodium pentobarbital overdose IP. The eyes with BSA-A647 were cryopreserved for confocal imaging analysis.[24] For BSA-preloading experiments, BSA without labeling was injected intravenously through the femoral vein, and then BSA-A647 was injected 5 minutes later.

Bovine serum albumin–GNPs were injected by catheterization of the left common carotid artery to obtain countable GNPs in mouse eyes, as determined in preliminary experiments. Mice were anesthetized with 0.15 mL ketamine/xylazine IP. A 1-cm midline, cervical skin incision was made with its caudal terminus at the level of the clavicle. The omohyoideus muscle was divided and retracted to visualize the left common carotid artery. The surgically isolated artery was ligated by nicking it and then inserting a catheter (0.014 outside diameter [OD] × 0.007 inner diameter [ID]) that was then tied in place. Three hundred microliters of BSA-GNP (5.0×10^{15} particles/mL) was injected using syringe pump (Sage Instruments; Orion Research, Inc., Jacksonsville, FL, USA) at a 0.02-mL/min flow rate ($n \geq 3$/group). After administration of 300 μL tracer, the animal was kept anesthetized for 5 minutes, perfused with PBS containing heparin, and then euthanized at 30 minutes after injection by IP sodium pentobarbital overdose. This time point was decided on because it is the time frame for uptake of albumen by ECs, and no gold was detected at longer time points. The concentration was chosen because higher concentrations and larger volumes induced stroke. To evaluate bulk vacuolar uptake of GNPs, GNPs with no BSA and GNPs coated with polyethylene glycol to neutralize surface charge were given to WT mice and processed after 30 minutes ($n = 3$ each). The eyes with gold probe were prepared for TEM, and the left eye only was analyzed because very little gold was found in the contralateral eye (Grebe R, unpublished results, 2015).

Tissue Collection and Labeling for Fluorescent Imaging

A Zeiss LSM 710 confocal microscopy (Carl Zeiss, Oberknochen, Germany) was used to evaluate the fluorescence distribution of injected BSA-A647 in the retina and choroid. Enucleated eyes were fixed 1 hour in 2% paraformaldehyde (PFA) in Tris-buffered saline (TBS) prior to the dissection of eyes and cryopreservation as previously reported,[25] followed by cross-sectional analysis. Cross-sections (8 μm) of tissues were washed with TBS containing 1% Triton X-100 for 1 hour, followed by incubation with *Griffonia simplicifolia* isolectin B4 conjugated to FITC (GS isolectin-FITC, 1:200; Invitrogen, Grand Island, NY, USA). Images were captured using a Zeiss LSM 710 confocal microscope (Carl Zeiss).

Analysis of BSA-A647 Relative Fluorescence

For a quantitative analysis of BSA-A647 distribution in CC, RPE, and photoreceptors (PRs), relative fluorescence values were determined from images (2048 × 2048 pixels) as illustrated in Figure 1. Fluorescent intensity was set to zero in tissue that had no tracer before measuring actual fluorescence from the dye to avoid the contribution of low level autofluorescence. Fluorescent intensity was measured using rectangular selections (20 × 60 pixels) of 15 separate fields of CC, RPE, and PRs from three sections per animal using the plot profile tool in ImageJ software as described previously.[26] A total of 45 measurements per animal were made for each structure. This was done for three mice from each time point and group captured under identical confocal microscope settings. The resulting numbers were averaged and expressed as corrected total fluorescence.

Transmission Electron Microscopy

Eyes for TEM analysis were fixed in 2.5% PFA/2% glutaraldehyde in 0.1 M cacodylate buffer, pH 7.4, for a minimum of 24 hours and processed as previously described.[27] Two 2.5-mm-long sections were cut from each block per grid, and five grids were made from each block. Images of three random areas in the section were captured. Five-nanometer gold was chosen because this size GNP could be distinguished from background electron dense particles. Gold is so electron-dense that the background can be thresholded away in Adobe Photoshop, leaving only 5-nm nonpixelated profiles of gold particles (Supplementary Fig. S4).

Statistical Analysis

Statistical analysis of corrected fluorescence intensity values was done using the paired Student's *t*-test with 2-tails, and $P \leq 0.05$ was considered significant.

Results

Alexa647-Conjugated BSA Transport by the Mouse Choriocapillaris

Free Alexa647 dye was completely removed from BSA-A647 solution by dialysis, which was corroborated by HPLC analysis, which showed a single peak with fluorescence and with UV (Supplementary Fig. S1). The fluorescently tagged albumen was then administered intravenously to young and aged mice. C57BL/6J (WT) mice that were 3 and 14 months of age were injected with 200 μL BSA-A647 containing 0.6 mg BSA, perfused with PBS, and killed at different time intervals after injection. In cryosections from eyes of young mice at 30 minutes after injection, A657-BSA fluorescence (red) was visible in the CC with a punctate pattern in choroidal blood vessels (Figs. 1A–1D). By 1 hour, most BSA labeling was still observed inside CC, which remained doubly labeled with GSA lectin (Figs. 1E–1H). By 4 hours, some of BSA-A647 was observed in RPE, and most had been cleared from choroid (Figs. 1I–1L). Bovine serum albumin–A647 was also observed in retina at 4 hours after injection (Fig. 1I).

Most BSA-A647 was observed in RPE, but some was outside retinal vessels in the eyes of aged WT mice at 30 minutes after injection (Fig. 2A). Notably, A647-BSA was clearly observed anterior to GSA isolectin labeling of CC already at this early

Investigative Ophthalmology & Visual Science

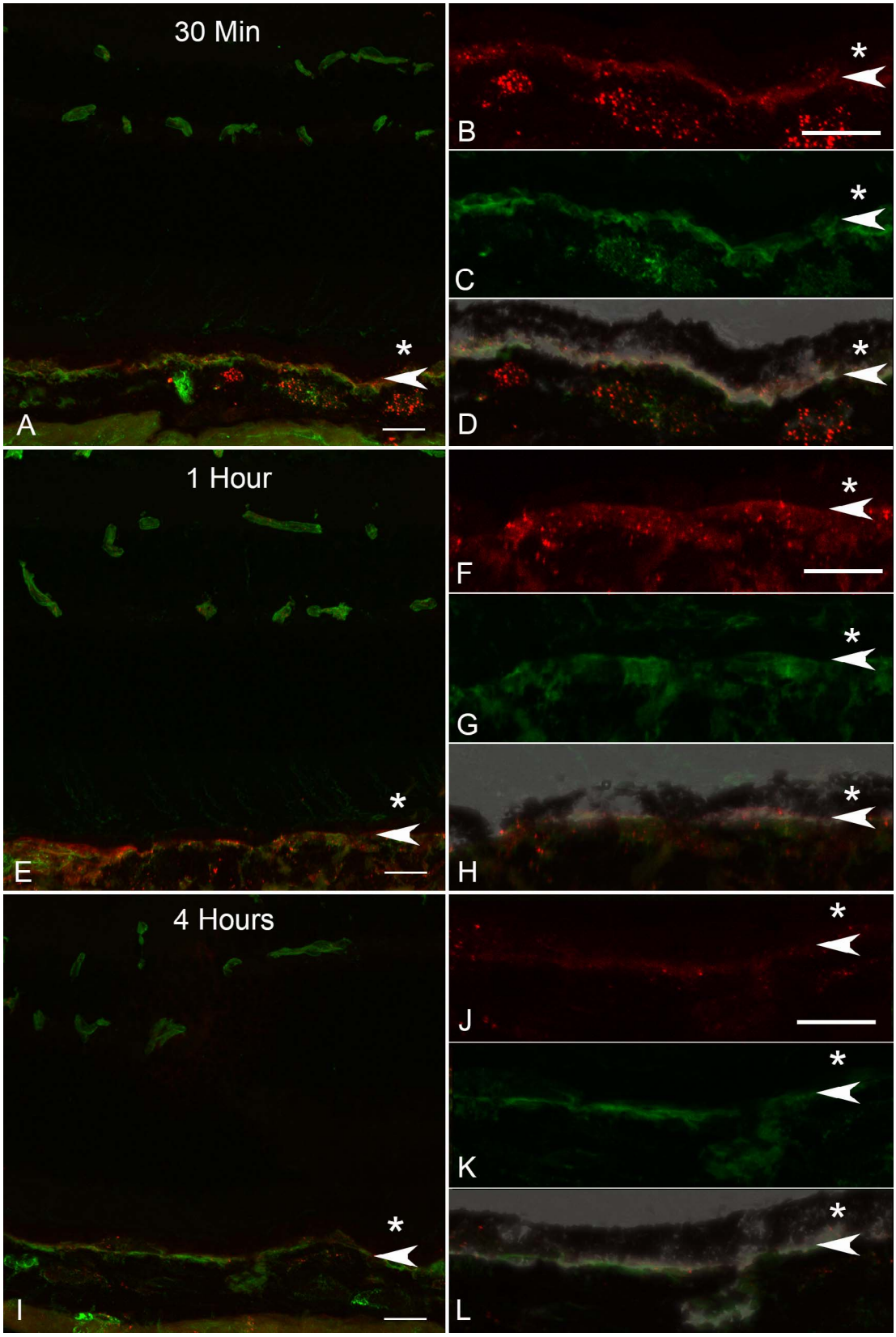

Figure 1. Albumen transport by choriocapillaris in 3-month-old WT mice. Cryosections of retina and choroid after intravenous injection of bovine serum albumen tagged with Alexa647 (BSA-A647; *red*). Blood vessels were labeled with GS isolectin-A488 (*green*). Animals were killed at 30 minutes (**A–D**), 1 hour (**E–H**), and 4 hours (**J–L**) after injection and imaged under identical conditions. In each panel, the *left* image has both colors merged, and on the *right*, at higher magnification, *red* (BSA) only, *green* (lectin) only, and merged colors with DIC are presented in succession. Over the time course, BSA-A647 appears to shift localization from CC to RPE (*asterisks* indicate RPE; *white arrowheads* indicate BM: *Scale bar*: 20 μm).

Investigative Ophthalmology & Visual Science

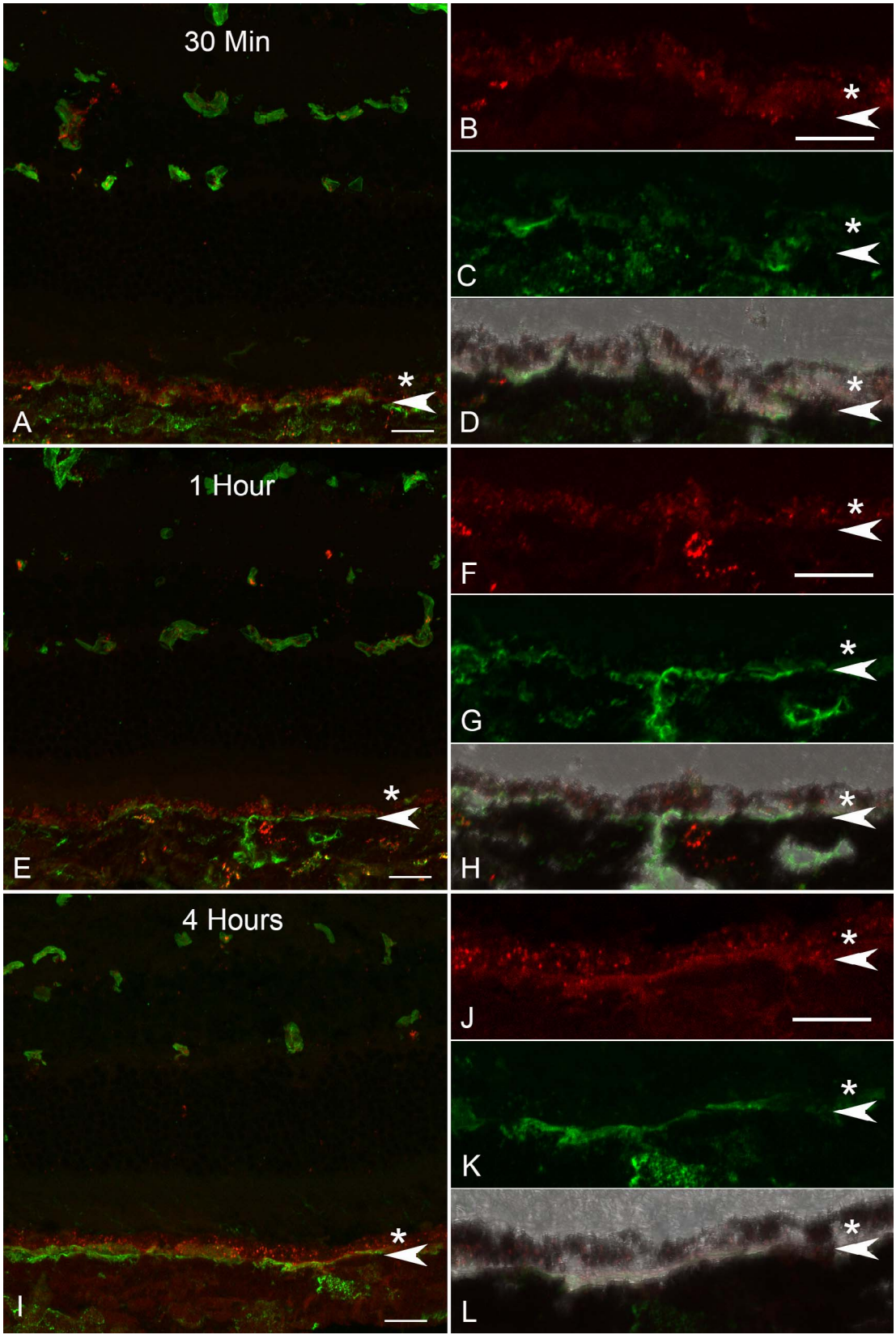

Figure 2. Bovine serum albumin–A647 was imaged at 30 minutes (**A–D**), 1 hour (**E–H**), and 4 hours (**J–L**) after injection in 14-month-old WT mice. In each panel, the *left* image has both colors merged, and then *red* (BSA) only, *green* (lectin) only, and merged colors with DIC presented in succession on the *right* at higher magnification. The RPE have significant BSA-A647 fluorescence even at 30 minutes after injection. There is abluminal BSA-A647 in retina at all time points (*asterisks* indicate RPE; *white arrowheads* indicate BM; *Scale bar*: 20 μm).

Investigative Ophthalmology & Visual Science

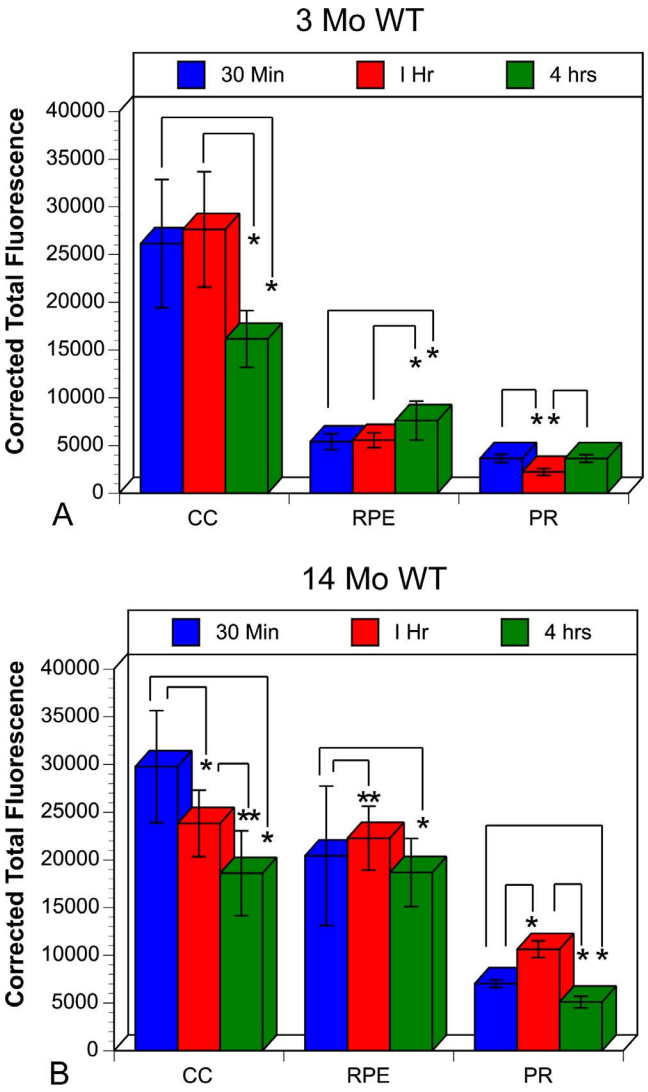

FIGURE 3. Tissue distribution of BSA-A647 in CC, RPE, and PRs in 3-month-old WT (**A**) and 14-month-old WT (**B**) as assessed by corrected total fluorescence intensity measurements made from images exemplified by images in Figures 1 and 2 (**$P < 0.01$; *$P < 0.001$).

time point. By 1 hour, diffuse weak fluorescence was observed in PR inner/outer segments, and RPE and CC remained labeled (Fig. 2B). By 4 hours, most of BSA remained visible in RPE (Fig. 2I). Albumenal BSA-A647 was observed in retina at all time points (Figs. 2A, 2E, 2I). The average fluorescence intensity of BSA-A647 in CC, RPE, and PRs is presented in Figure 3, where values for young and aged mice are compared.

Tissue Distribution of BSA-GNP in CC of Young and Aged WT Mice

To analyze the tissue and cellular distribution of albumen in mouse choroid, gold nanoparticles were selected as tracers for TEM. These are a bio-inert colloidal suspension with a variety of nanometer sizes, which can be synthesized under the precise size control with a low polydispersity.[28] The BSA-GNP had a 12.1-nm hydrodynamic diameter with a unimodal distribution, as determined by Zeta sizer (Supplementary Fig. S2). The surface of BSA-GNP was negatively charged, and its charge was closer to BSA than to naked GNP. The TEM analysis showed that GNPs were successfully coated by a BSA corona, which was consistent with the zeta-potential analysis, and BSA-GNPs did not aggregate (Supplementary Fig. S3). Bovine serum albumin–GNPs were administrated through the left common carotid artery to supply sufficient tracers to the CC, at least in the eye on the side of the injection. We found that no BSA-GNP reached the contralateral eye (right eye; data not shown).

In young WT mice after 30 minutes of circulation, BSA-GNPs were observed in caveolae of ECs in most areas of CC (Figs. 4A, 4B). The caveolae with BSA-GNP were on the luminal surface, within the EC soma, and released into the perivascular milieu (Figs. 4C, 4D), that is, they were transcytosed by the EC via caveolae. Some BSA-GNPs were also found in BM (Figs. 4C, 4D).

The tissue distribution observed in aged WT mice was similar to young WT, but BSA-GNPs were also found in other compartments of the CC/BM/RPE complex. Bovine serum albumin–GNPs were observed in caveolae of CC ECs and also were released into BM (Fig. 5A). Interestingly, a large number of BSA-GNPs were retained at the luminal orifice of fenestrations and appeared to be confined to the luminal side by the diaphragm of fenestrations (Figs. 5A, 5B). Rarely were they found on the abluminal side of the fenestration pore, even after perfusion (Fig. 5). In addition, clusters of BSA-GNPs were found in between the leaflets of ECs at loose or incomplete TJs (Figs. 5B, 5C). Transendothelial channels also transported BSA-GNPs from lumen (Fig. 5B). Also, a substantial number of BSA-GNPs were transported to RPE basal infoldings at this time point (Fig. 5D). Gold nanoparticles without BSA and GNPs that were coated with polyethylene glycol to neutralize the surface charge were not taken up by caveolae and not found in the CC lumens (Supplementary Fig. S5). Therefore, serum albumen in old and young WT mice was predominantly transported from endothelial cells to BM via caveolae-mediated transcytosis and not via fenestrations or bulk vacuolar transport.

Transport of BSA-A647 in the Eye of Young Cav1$^{-/-}$

To further investigate the caveolae-mediated transport of BSA, BSA-A647 and BSA-GNPs were administrated under the same conditions as WT mice to 3-month-old *Cav1*$^{-/-}$ mice, which lack caveolae. Thirty minutes after injection, BSA-A647 was primarily localized to the BM side of CC but the punctate fluorescence found in WT was less visible in *Cav1*$^{-/-}$ mice (Fig. 6). At 1 hour, BSA-A647 remained associated with CC (data not shown). By 4 hours, BSA-A647 had not been cleared from CC as it had been in the WT, and the pattern of the BSA-A647 in CC remained the same as other time points; however, it was reduced in CC at 4 hours (Fig. 6B) but not to the extent that it was reduced in the WT mice at 4 hours (Fig. 3). The level did not increase significantly in RPE at 1 or 4 hours as it had in the WT. This observation suggested that albumen in *Cav1*$^{-/-}$ was bound to gp60, the albumen receptor, but the transcytosis process of albumen-gp60 did not occur. Therefore, it was assumed that the fluorescent layer was probably the aggregate of albumen–gp60 complex that remained on the *Cav1*$^{-/-}$ endothelial cell surface. Also, of interest, fluorescent signal from BSA-A647 was rarely observed in retina at any of the three time points but it was in the control mice.

Tissue Distribution of BSA-GNPs in CC of Cav1$^{-/-}$

Bovine serum albumin–GNPs were administered to 3-month-old *Cav1*$^{-/-}$ mice, and the animals were killed 30 minutes after the start of injection, as in the WT mice. The majority of the BSA-GNPs were observed on the luminal surface of the ECs (Fig. 7). However, some BSA-GNPs were observed in vesicles forming at the surface of the CC ECs (Fig. 7C) and occasionally

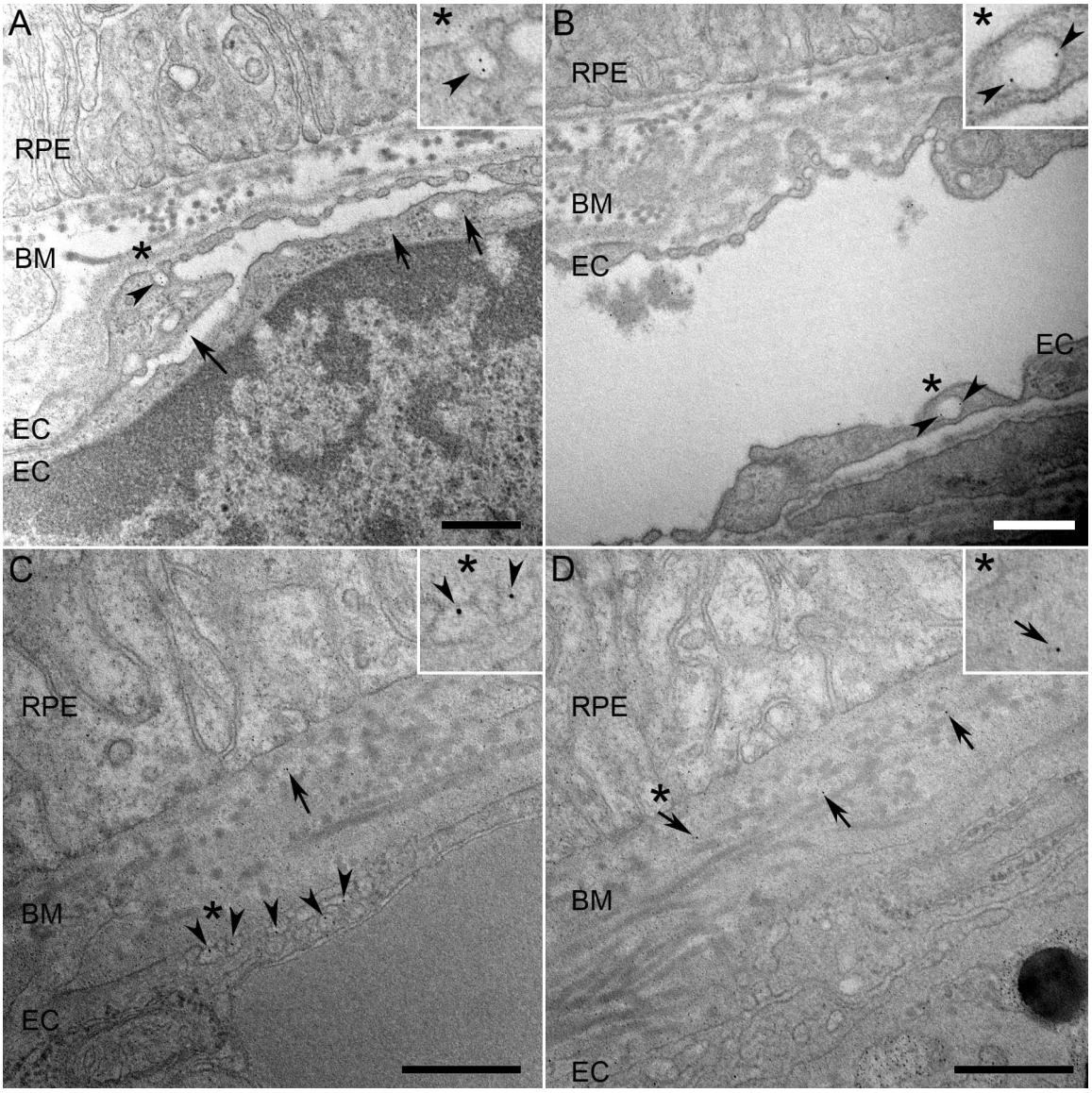

Figure 4. Ultrastructural distribution of BSA-GNPs (*arrows* and *arrowheads*) in the CC/BM/RPE complex of the left eyes of 3-month-old WT mice when animals were killed at 30 minutes after injection. (**A**) Bovine serum albumin–GNPs were present in caveolae with diaphragm on the abluminal EC surface (*arrowheads*), on the EC luminal surface (*long arrow*), and in EC cytosol (*short arrows*). (**B**) Bovine serum albumin–GNPs were present in EC caveolae (*arrowheads* and *insets*) on the scleral side of CC. (**C**) Bovine serum albumin–GNPs were present in caveolae open to the abluminal surface of ECs (*arrowheads*) and in BM (*arrows*). (**D**) Bovine serum albumin–GNPs (*arrows*) in BM 30 min after injection (*insets* show magnified area labeled with *asterisk* in all; *Scale bar*: 500 nm).

within vesicles in the ECs, whereas others were free in the cytoplasm of the CC (Fig. 7D). Rarely were BSA-GNPs observed in RPE basal infoldings (Fig. 7A) or BM. Those rare BSA-GNPs in the BM may have diffused through the open TJs that we and others have observed in *Cav1*$^{-/-}$ mice (Fig. 7A).[29]

Effect of Albumen Receptor Saturation BSA transport

As further evidence for BSA binding to its gp60 receptor on CC, the receptors were saturated with unlabeled BSA before administering BSA-A647 to WT and *Cav1*$^{-/-}$. We hypothesized that BSA-A647 would remain on the cell surface of endothelium as a complex formed with gp60 receptor in *Cav1*$^{-/-}$, but the tracer would be internalized in the WT where new, unsaturated receptors would have cycled to the surface. The unlabeled BSA was administered via the common carotid artery to avoid loss of all BSA in the rest of the body. The BSA-A647 was administered 5 minutes after injection of BSA, and only the eye on the side injected with BSA was analyzed. As predicted, no BSA-A647 was observed at the surface of CC in *Cav1*$^{-/-}$ after saturating the gp60 on the surface of the CC ECs (Fig. 8). However, BSA-A647 was prominent at the surface of the WT mice (Figs. 8A, 8C, 8E), presumably because new gp60 receptors were shuttled to the cell membrane on the luminal surface.

Discussion

The CC is responsible for supplying nutrients to RPE and PRs, as well as removing waste from the RPE. This is accomplished by several transport systems: fenestrations, caveolae, and

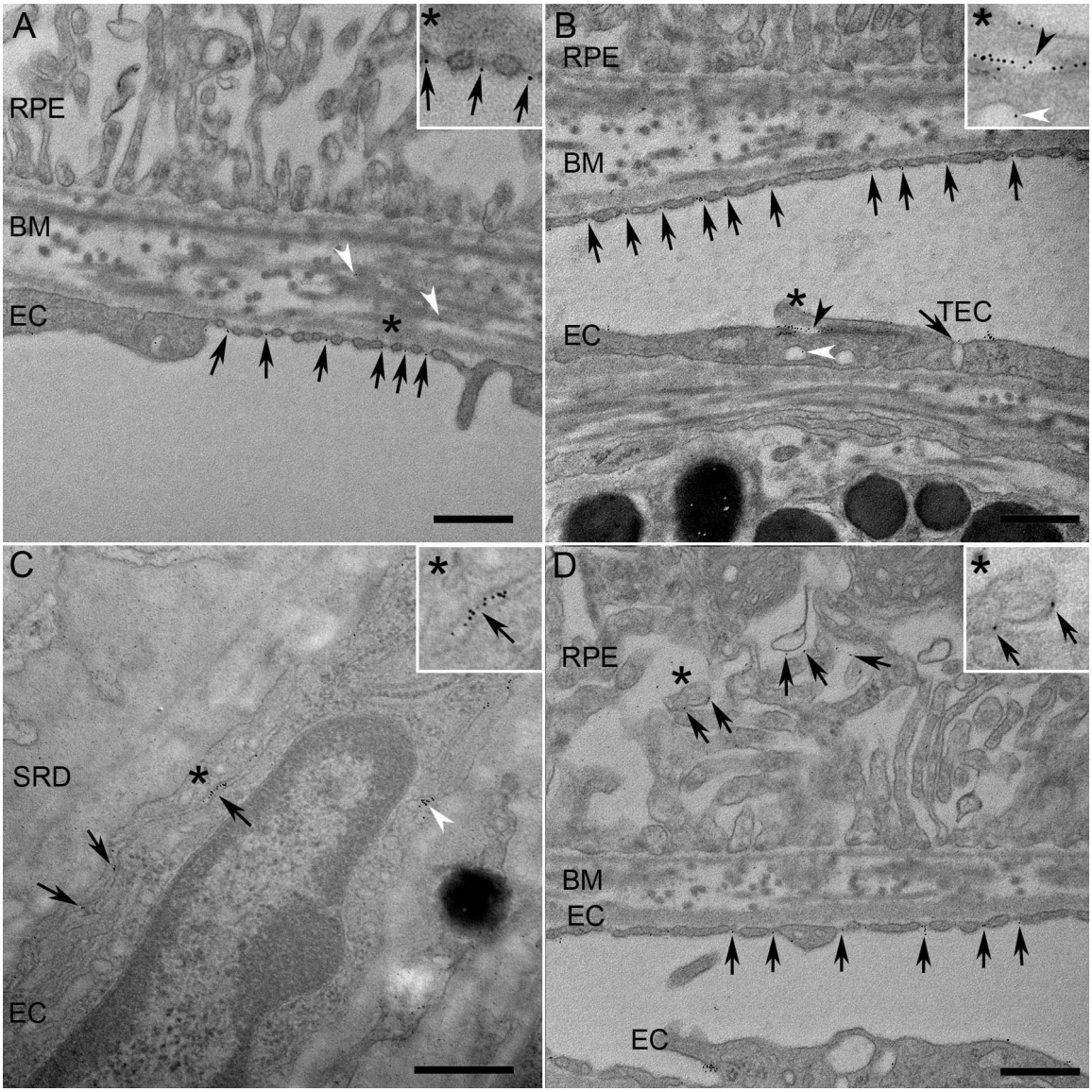

Figure 5. Ultrastructural distribution of BSA-GNP in CC/BM/RPE complex of aged (14 months) WT mice at 30 minutes after injection. (**A**) Bovine serum albumin–GNPs were present at the opening to the fenestrations on the luminal side (*black arrows*) and in BM (*white arrowheads*). (**B**) Bovine serum albumin–GNPs were present in open tight junctions (*black arrowhead*), as well as at the luminal orifice of a TEC, fenestrations (*arrows*), and caveolae (*white arrowhead*). (**C**) A cluster of BSA-GNPs (*black arrows*) is in the constricted CC lumen and caveolae adjacent to a pericyte (*white arrowhead*). (**D**) Bovine serum albumin–GNPs (*black arrows*) were at fenestrations and even in RPE basal infoldings at 30 minutes after injection (*insets* show magnified area labeled with *asterisk* in all; *Scale bar*: 500 nm; SRD, subretinal deposit).

receptor-mediated endocytosis. The current study focused on transport of just one serum macromolecule: albumen. Albumen was chosen because of its abundance, its globular shape with an approximate molecular weight of 68 kDa, and its importance in maintaining oncotic pressure of plasma, as well as the fact that it is not glycosylated. It is also a carrier of steroids, fatty acids, and thyroid hormones. Albumen is negatively charged so it is not attracted to normal EC glycocalyx, which is also negatively charged. Although albumen transport has been studied extensively in kidney and other organs, it has never been studied in CC. Using both a fluorescent and an electron dense albumen complex, the current study demonstrated that the majority of albumen is transported across the CC by transcytosis via caveolae and not through the CC fenestrations.

Caveolae were first described by Palade et al. who called them plasmalemma vesicles[30] and Yamada who called them caveolae (little caves).[31] Caveolae are the vesicular carriers filled with receptor-bound and unbound free solutes that are shuttled between the vascular and extravascular spaces, being deposited outside the cell. The caveolae contain receptors for many ligands[7,32] including serum albumen (Table).[9] Two tracers were used for this study: BSA-GNP and BSA-A647. The GNP-conjugated BSA is orders of magnitude larger than the BSA-A647, but the time course and route of uptake appeared similar. At 30 minutes, BSA-GNPs were observed in caveolae in young WT mice and BSA-A647 was in CC. When caveolae were absent in *Cav1*$^{-/-}$ mice, no uptake of BSA-A647 was observed. Also, the uptake by HUVECS of BSA-A647 but not A647 occurred so labeling did not affect uptake by ECs, and it was observed in a perinuclear compartment, perhaps Golgi or endoplasmic reticulum (Supplementary Fig. S6), sites of caveolae trafficking.[33] Therefore, the disparate size of the

Investigative Ophthalmology & Visual Science

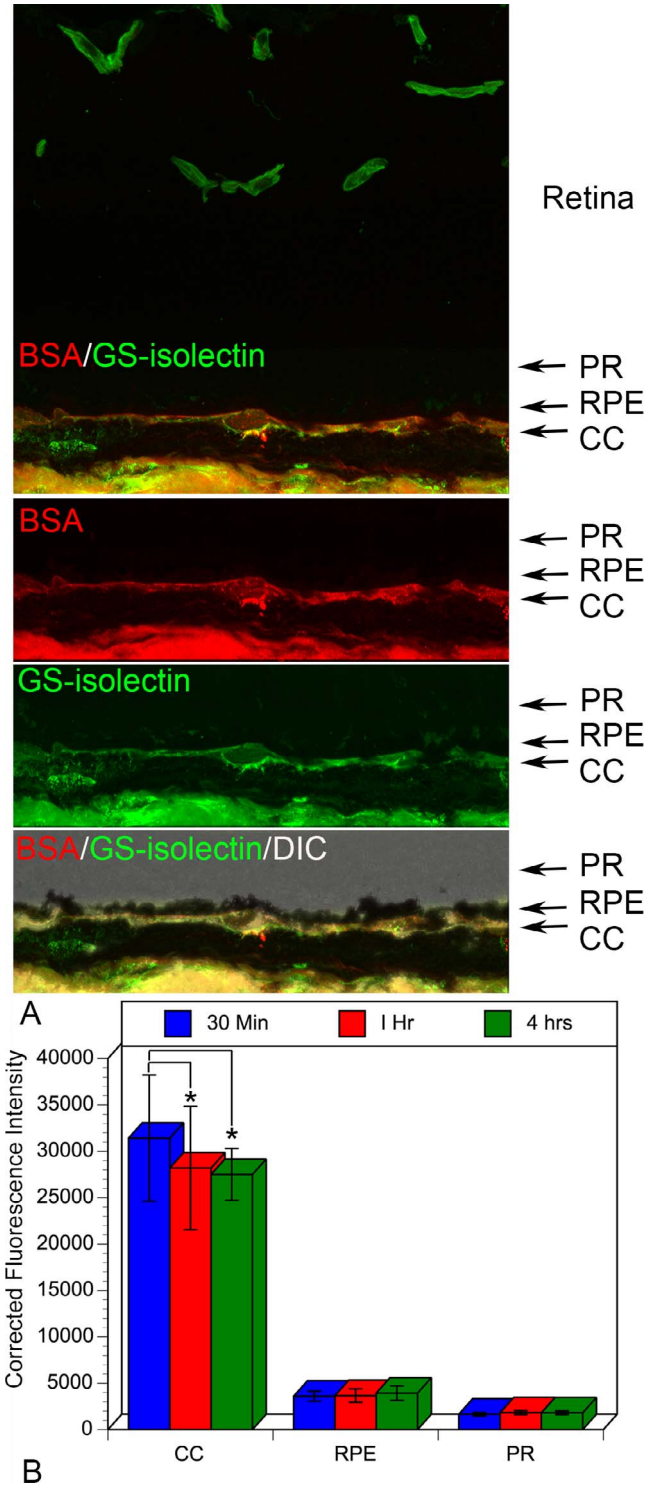

Figure 6. Albumen transport in 3-month-old Cav1$^{-/-}$ mice. (**A**) Cryosections of retina and choroid after intravenous injection of BSA-A647 (*red*), and blood vessels were labeled with FITC-GS isolectin (*green*). After 4 hours, the BSA still remains primarily restricted to the CC. (**B**) Tissue distribution of BSA-A647 in CC, RPE, and PR at 30 minutes, 1 hour, and 4 hours after injection expressed as corrected total fluorescence intensity from measurement made from images as shown in **A** (*$P < 0.001$).

tracers used in this study did not appear to have altered the route of albumen transcytosis by ECs.

By 4 hours in young WT mice, the BSA-A647 was cleared from CC and was present in the BM and RPE. Furthermore, preloading the CC with nonlabeled BSA prevented uptake in Cav1$^{-/-}$ mice; this demonstrated that the uptake was probably via binding to the albumen gp60 receptor, which is known to be responsible for receptor-mediated albumen caveolae transport.[34–36] Gold nanoparticles without BSA and GNPs that were coated with polyethylene glycol to neutralize the surface charge were not taken up by caveolae and not found in the CC lumens (Supplementary Fig. S5). Therefore, bulk vacuolar uptake of plasma constituents was not responsible for uptake by CC, and binding to receptors by BSA-GNPs was required for uptake.

Caveolae are found in retinal and choroidal capillary ECs, as well as pericytes. Therefore, albumin transcytosis can occur in either vasculature. The BSA-A647 for photoreceptors could come from transcytosis by the retinal or choroidal vasculature. Although BSA-A647 was observed bound to or within retinal ECs at 1 hour in young WT mice, it was not observed abluminally until 4 hours. In old WT mice, abluminal retinal BSA-A647 was observed at all time points (Fig. 2). Our studies can not quantitatively prove the origin of BSA-A647 in the PRs, but the relative fluorescence and timing of BSA-A647 transport from CC suggests that CC and not retinal ECs is the source in young WT mice. *Cav*$^{-/-}$ mice were used to further evaluate the contribution of caveolae to albumen transcytosis. These mice lack caveolae and have impaired nitric oxide and calcium signaling, thickening of lung alveoli, and EC dysfunction.[37,38] Bovine serum albumin–A647 injected into *Cav*$^{-/-}$ mice localized to the luminal side of CC in *Cav*$^{-/-}$ but was never transported to the RPE or BM. The BSA-GNPs, however, were observed in some large vesicles within the ECs and in cytosol. This may represent an alternative pathway for endocytosis, but interestingly appeared not to transport BSA to BM and RPE. The vesicles were never seen at the abluminal surface of the EC, indicating the BSA-GNPs were not transported to the BM and RPE in *Cav1*$^{-/-}$. Stan et al. observed these vesicles in the liver of *Cav1*$^{-/-}$ mice.[6] In the animals preloaded with nonlabeled BSA, the BSA-A647 fluorescent layer was not visible in CC of *Cav1*$^{-/-}$, whereas there was BSA-A647 in CC of WT mice. These data suggest that all gp60 on the surface of the EC in *Cav1*$^{-/-}$ mice were saturated with nonlabeled BSA. However, in the WT mice the saturated receptors were likely internalized and new gp60 receptors had apparently come to the surface by the time the BSA-A647 was administered (Fig. 7A). These findings support our hypothesis that the albumen–gp60 complex is not internalized without caveolin-1; therefore, serum albumen is transported from luminal side to BM via caveolae-mediated transcytosis in CC.

The aging process affected BSA transport by CC. In aged WT mice, both tracers were observed in RPE in 30 minutes, and a fluorescent layer of uniformly diffuse albumen was visible in photoreceptor area by 1 hour after injection. Even though albumen was transported more rapidly to BM and RPE in aged mice compared with young WT, BSA-A647 remained in CC longer in aged mice (4-hour time point; Fig. 2) than in young mice (Fig. 1). Further analysis of the aged WT CC with TEM demonstrated that gold had accumulated between the EC leaflets; in other words, between the thin processes where ECs overlap and form TJs. Open TJs were also observed in aged WT, suggesting that leakage of albumen may have occurred in old WT mice. In fact, BSA-GNPs were observed leaking from retinal vessel in aged WT mice (data not shown). The more rapid transport of albumen, the presence of BSA-GNPs between EC leaflets, and apparent leakage of albumen from retinal vessels

Investigative Ophthalmology & Visual Science

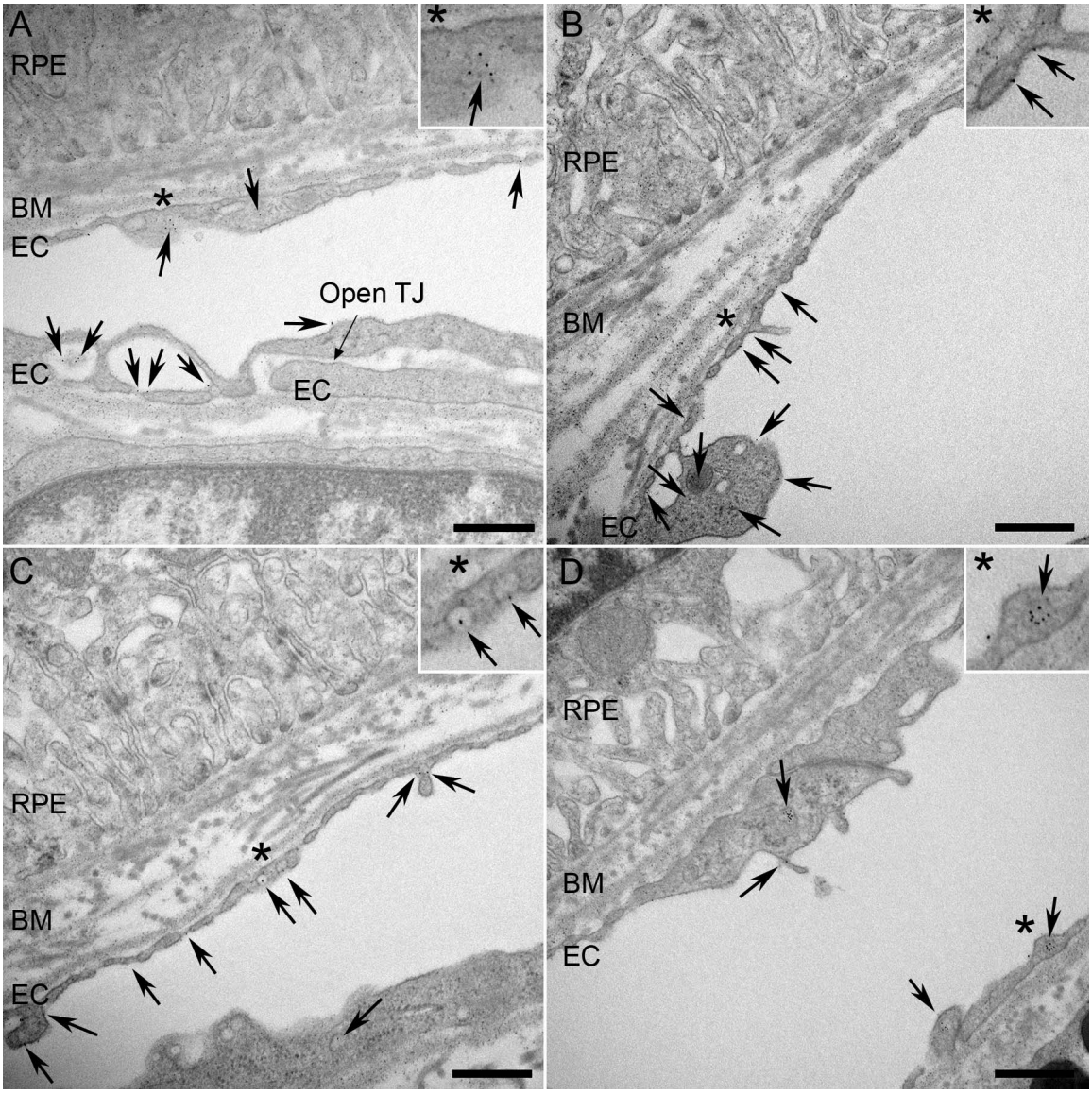

Figure 7. Ultrastructural distribution of BSA-GNPs (*arrows*) in the CC/BM/RPE complex in 3-month-old *Cav1*$^{-/-}$ mice at 30 minutes after injection. (**A**) Bovine serum albumin–GNPs (*arrow*) were present at the luminal surface and intracellular but not confined to vesicles. There were open tight junctions (open TJ) in some CC. (**B**) Bovine serum albumin–GNPs (*arrows*) were on the luminal surface of ECs (*asterisk* and *inset*) and in cytoplasm of ECs. (**C**) Some vesicles formed at the luminal surface (*asterisk* and *inset*), but none were found abluminally. (**D**) Bovine serum albumin–GNPs (*arrows*) were present in cytoplasm but not confined to vesicles (*black arrows*, BSA-GNP; *insets* show magnified area labeled with *asterisk* in all; *Scale bar*: 500 nm).

suggest that tight regulation of transport by CC and retinal blood vessels is reduced in aging.

Although fenestrations do not appear to transport albumen, it is worth discussing their role in CC and the changes observed in them with age. Fenestrations are 60–80 nm in diameter, but the CC fenestrations have diaphragms, which divide the pore yielding a predicted opening of 6 nm (Table). In addition, the opening to the pore is covered in a negatively charged glycocalyx.[12,13] Bovine serum albumin–GNPs were observed on the luminal side of fenestrations in aged mice but never transported to the abluminal space adjacent to fenestrations (Fig. 5). Bovine serum albumin–GNPs remaining on the luminal side of the fenestration pores after perfusion suggest that the glycocalyx on diaphragm of fenestrations captured BSA-GNP. Therefore, the localization changed during aging, and fenestrations of aged ECs do not function as transport system for albumen even when the albumen is bound to the luminal pore opening due to size exclusion imposed by diaphragms. Therefore, it appears that the glycocalyx over the fenestration diaphragms may change in aging as has been observed in fenestrated capillary beds during diabetes.[39]

Tight junctions are junctions between the leaflets of adjacent ECs, which prevent leakage of materials between endothelial cells. The molecules in the TJs are known to denature with age, which can cause leakage of serum proteins between adjacent EC.[40] Transmission electron microscopy imaging demonstrated that loose TJs of ECs had BSA-GNP aggregation in CC of aged WT mice (Fig. 5). This observation explains the more rapid transport of albumen in aged WT mice compared with in young WT (Figs. 1, 2). In addition to choroid, this observation is consistent with albumen transport in retina. Whereas the fluorescence signal from injected BSA-A647 was observed outside of retinal vessels by 4 hours in young WT (Fig. 1C), it occurred in aged WT by 30 minutes (Fig.

Investigative Ophthalmology & Visual Science

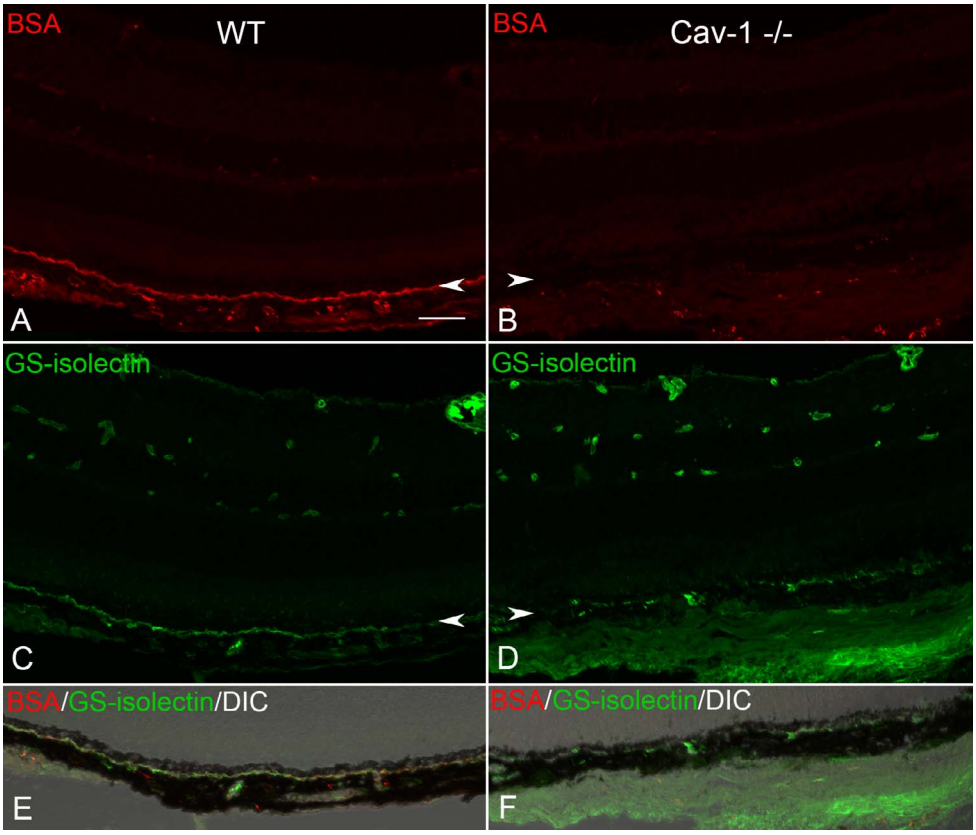

Figure 8. Fluorescently-tagged albumen (BSA-A647; *red*) uptake by CC in eyes of 3-month-old WT (**A**, **C**, **E**) and *Cav1*$^{-/-}$ (**B**, **D**, **F**) mice after preloading with excess BSA via the left carotid common artery. Mice were injected intravenously with 3 mg BSA, and then 5 minutes later received BSA-A647. Mice were perfused and killed at 30 minutes after injection of BSA-A647. Cryosections were imaged under the identical conditions. Blood vessels were labeled with GS isolectin-AF488 (*green*). (**A**) Bovine serum albumin–A647 was localized to CC in WT. (**B**) No BSA-A647 was associated with the CC in the *Cav1*$^{-/-}$ (*Scale bar*: 20 μm).

1D). These findings demonstrated that aged mice have open TJs, resulting in loss of regulation and control of albumen transport.

In summary, the CC is an understudied vasculature responsible for transport to and from the RPE and PRs. Detailed analysis by TEM in mice indicates that CC transport of albumen is performed mainly by caveolae and TEC and not by fenestrations. The proteomics study on aged and AMD BM/choroid tissue in aging and AMD human subjects by Yuan et al. reported serum proteins like erythrocyte-specific proteins and von Willebrand factor in BM and choroid that are not known to be transported by CC.[41] Our observation of increased and uncontrolled transport (through open TJs) of BSA from aged CC could explain the observation of Yuan et al. If CC transport is dysfunctional in AMD, it could yield accumulation of serum proteins in choroid, inadequate removal of material from RPE, and poor transport of materials to RPE and retina. Understanding the mechanisms of CC transcytosis and how they are altered in diseases could be invaluable for designing systemic therapies.

Acknowledgments

Supported by National Eye Institute Grants EY-01765 (Wilmer) and R01-EY016151 (GAL), unrestricted funds from Research to Prevent Blindness (Wilmer), the Foundation Fighting Blindness (GAL), and the Altsheler Durell Foundation.

Disclosure: **M. Nakanishi**, None; **R. Grebe**, None; **I.A. Bhutto**, None; **M. Edwards**, None; **D.S. McLeod**, None; **G.A. Lutty**, None

References

1. Wangsa-Wirawan ND, Linsenmeier RA. Retinal oxygen. Fundamental and clinical aspects. *Arch. Ophthalmol*. 2003;121:547–557.
2. Pino RM. Restriction to endogenous plasma proteins by a fenestrated capillary endothelium: an ultrastructural immunocytochemical study of the choriocapillary endothelium. *Am J Anat*. 1985;172:279–289.
3. Bernstein MH, Hollenberg MJ. Fine structure of the choriocappillaris and retinal capillaries. *Invest Ophthalmol Vis Sci*. 1965;4:1016–1025.
4. Braet F, Wisse E. Structural and functional aspects of liver sinusoidal endothelial cell fenestrae: a review. *Comp Hepatol*. 2002;1:1–29.
5. Satchell SC, Braet F. Glomerular endothelial cell fenestrations: an integral component of glomerular filtration barrier. *Am J Physiol Renal Physiol*. 2008;296:947–956.
6. Stan RV. Structure of caveolae. *Biochim Biophys Acta*. 2005;1746:334–348.
7. Simionescu M, Gafencu A, Antohe F. Transcytosis of plasma macromolecules in endothelial cells: a cell biological survey. *Microsc Res Tech*. 2002;57:269–288.
8. Stan RV. Endocytosis pathways in endothelium: how many? *Am J Physiol Lung Cell Mol Physiol*. 2006;290:L806–L808.
9. Anderson RG. The caveolae membrane system. *Annu Rev Biochem*. 1998;67:199–225.
10. Botos E, Klumperman J, Oorschot V, et al. Caveolin-1 is transported to multi-vesicular bodies after albumin-induced

endocytosis of caveolae in HepG2 cells. *J Cell Mol Med*. 2008; 12:1632–1639.

11. Bearer EL, Orci L. Endothelial fenestral diaphragms: a quick-freeze, deep-etch study. *J Cell Biol*. 1985;100:418–428.
12. Arkill KP, Knupp C, Michel CC, et al. Similar endothelial glycocalyx structures in microvessels from a range of mammalian tissues: evidence for a common filtering mechanism? *Biophys J*. 2011;101:1046–1056.
13. Arkill KP, Neal CR, Mantell JM, et al. 3D reconstruction of the glycocalyx structure in mammalian capillaries using electron tomography. *Microcirculation*. 2012;19:343–351.
14. Ichimura K, Stan RV, Kurihara H, Sakai T. Glomerular endothelial cells form diaphragms during development and pathologic conditions. *J Am Soc Nephrol*. 2008;19:1463–1471.
15. Stan RV, Kubitza M, Palade GE. PV-1 is a component of the fenestral and stomatal diaphragms in fenestrated endothelia. *Proc Natl Acad Sci U S A*. 1999;96:13203–13207.
16. Stan RV, Tkachenko E, Niesman IR. PV1 is a key structural component for the formation of the stomatal and fenestral diaphragms. *Mol Biol Cell*. 2004;15:3615–3630.
17. Aiello LP, Gardner TW, King GL, et al. Diabetic retinopathy. *Diabetes Care*. 1998;21:143–156.
18. Pino RM, Essner E. Structure and permeability to ferritin of the choriocapillary endothelium of the rat eye. *Cell Tissue Res*. 1980;208:21–27.
19. Pino RM, Essner E. Permeability of rat choriocapillaris to hemeproteins. Restriction of tracers by a fenestrated endothelium. *J Histochem Cytochem*. 1981;29:281–290.
20. Pino RM, Essner E, Pino LC. Permeability of the neonatal rat choriocapillaris to hemeproteins and ferritin. *Am J Anat*. 1982;164:333–341.
21. Pino RM, Thouron CL. Vascular permeability in the rat eye to endogenous albumin and immunoglobulin G (IgG) examined by immunohistochemical techniques. *J. Histochem. Cytochem*. 1983;31:411–416.
22. Pino RM. Restriction of exogenous transthyretin (prealbumin) by the endothelium of the rat choriocapillaris. *Am J Anat*. 1986;177:63–70.
23. Pino RM. Binding and endocytosis of heparin-gold conjugates by the fenestrated endothelium of the rat choriocapillaris. *Cell Tissue Res*. 1987;250:257–266.
24. Hasegawa T, McLeod DS, Bhutto IA, et al. The embryonic human choriocapillaris develops by hemo-vasculogenesis. *Dev Dyn*. 2007;236:2089–2100.
25. Lutty GA, Merges C, Threlkeld AB, Crone S, McLeod DS. Heterogeneity in localization of isoforms of TGF-b in human retina, vitreous, and choroid. *Invest. Ophthalmol. Vis. Sci*. 1993;34:477–487.
26. Hartig SM. Basic image analysis and manipulation in ImageJ. *Curr Protoc Mol Biol*. 2013;102:1–14.
27. Baba T, Grebe R, Hasegawa T, et al. Maturation of the fetal human choriocapillaris. *Invest Ophthalmol Vis Sci*. 2009;50: 3503–3511.
28. Slyusarenko K, Abecassis B, Davidson P, Constantin D. Morphology of gold nanoparticles determined by full-curve fitting of the light absorption spectrum. Comparison with X-ray scattering and electron microscopy data. *Nanoscale*. 2014; 6:13527–13534.
29. Schubert W, Frank PG, Woodman SE, et al. Microvascular hyperpermeability in caveolin-1 (-/-) knock-out mice. Treatment with a specific nitric-oxide synthase inhibitor, L-NAME, restores normal microvascular permeability in Cav-1 null mice. *J Biol Chem*. 2002;277:40091–40098.
30. Predescu SA, Predescu DN, Palade GE. Plasmalemmal vesicles function as transcytotic carriers for small proteins in the continuous endothelium. *Am J Physiol*. 1997;272:H937–H949.
31. Yamada E. The fine structure of the renal glomerulus of the mouse. *J Histochem Cytochem*. 1955;3:309–320.
32. Predescu SA, Predescu DN, Malik AB. Molecular determinants of endothelial transcytosis and their role in endothelial permeability. *Am J Physiol Lung Cell Mol Physiol*. 2007;293: L823–L842.
33. Carver LA, Schnitzer JE. Caveolae: mining little caves for new cancer targets. *Nat Rev Cancer*. 2003;3:571–581.
34. Schnitzer JE, Ulmer JB, Palade GE. A major endothelial plasmalemmal sialoglycoprotein, gp60, is immunologically related to glycophorin. *Proc Natl Acad Sci U S A*. 1990;87: 6843–6847.
35. Schnitzer JE. gp60 is an albumin-binding glycoprotein expressed by continuous endothelium involved in albumin transcytosis. *Am J Physiol*. 1992;262:H246–H254.
36. Siflinger-Birnboim A, Schnitzer J, Lum H, et al. Lectin binding to gp60 decreases specific albumin binding and transport in pulmonary artery endothelial monolayers. *J Cell Physiol*. 1991; 149:575–584.
37. Drab M, Verkade P, Elger M, et al. Loss of caveolae, vascular dysfunction, and pulmonary defects in caveolin-1 gene-disrupted mice. *Science*. 2001;293:2449–2452.
38. Schubert W, Frank PG, Razani B, Park DS, Chow CW, Lisanti MP. Caveolae-deficient endothelial cells show defects in the uptake and transport of albumin in vivo. *J Biol Chem*. 2001; 276:48619–48622.
39. Gilbert RE. The endothelium in diabetic nephropathy. *Curr Atheroscler Rep*. 2014;16:410.
40. Elahy M, Jackaman C, Mamo JC, et al. Blood-brain barrier dysfunction developed during normal aging is associated with inflammation and loss of tight junctions but not with leukocyte recruitment. *Immun Ageing*. 2015;12:2.
41. Yuan X, Gu X, Crabb JS, et al. Quantitative proteomics: comparison of the macular Bruch membrane/choroid complex from age-related macular degeneration and normal eyes. *Mol Cell Proteomics*. 2010;9:1031–1046.
42. Sarin H. Physiologic upper limits of pore size of different blood capillary types and another perspective on the dual pore theory of microvascular permeability. *J Angiogenes Res*. 2010; 2:14–19.
43. Mann GE, Smaje LH, Yudilevich DL. Epithelial uptake of vitamin B12 in the cat salivary gland [proceedings]. *J Physiol*. 1978;285:32P.
44. Mann GE, Smaje LH, Yudilevich DL. Permeability of the fenestrated capillaries in the cat submandibular gland to lipid-insoluble molecules. *J Physiol*. 1979;297:335–354.
45. Smith SS, Pino RM, Thouron CL. Binding and transport of transthyretin-gold by the endothelium of the rat choriocapillaris. *J Histochem Cytochem*. 1989;37:1497–1502.
46. Goldstein JL, Anderson RG, Brown MS. Coated pits, coated vesicles, and receptor-mediated endocytosis. *Nature*. 1979; 279:679–685.

Investigative Ophthalmology & Visual Science